NASA CONTRACTOR REPORT

NASA CR-2284

NASA CR-2284

LASER DOPPLER VELOCITY MEASUREMENTS OF SWIRLING FLOWS WITH UPSTREAM INFLUENCE

by Kenneth L. Orloff and Hartmut H. Bossel

Prepared by
UNIVERSITY OF CALIFORNIA
Santa Barbara, Calif. 93106
for Langley Research Center

NATIONAL AERONAUTICS AND SPACE ADMINISTRATION • WASHINGTON, D. C. • JULY 1973

1. Report No.	2. Government Accession No.	3. Recipient's Catalog No.
NASA CR-2284		

4. Title and Subtitle	5. Report Date
LASER DOPPLER VELOCITY MEASUREMENTS OF SWIRLING FLOWS WITH UPSTREAM INFLUENCE	July 1973
	6. Performing Organization Code

7. Author(s)	8. Performing Organization Report No.
Kenneth L. Orloff and Hartmut H. Bossel	

9. Performing Organization Name and Address	10. Work Unit No.
University of California, Santa Barbara, California 93106	501-06-04-01
	11. Contract or Grant No. NGR 05-010-025
	13. Type of Report and Period Covered Contractor Report

12. Sponsoring Agency Name and Address	14. Sponsoring Agency Code
National Aeronautics and Space Administration Washington, D.C. 20546	

15. Supplementary Notes

16. Abstract

Swirling flow in a rotating tube is studied by flow visualization at a moderate Reynolds number, and its velocity field is measured by laser-Doppler anemometry. The tube has constant diameter, and approximately uniform initial rigid rotation of the flow is assured by passing the flow through a rotating plug of porous metal before it enters the test section. At moderate swirl values, an object mounted on the tube centerline causes a closed bubble to form upstream of the obstacle, with a clearly defined stagnation point on the axis, and recirculating flow inside the bubble. The bubble length grows upstream as the swirl is increased, until it breaks up into a Taylor column reaching all the way upstream and downstream at swirl values above a certain critical value. A vortex jump (in the sense of Benjamin) occurs downstream of the obstacle except when the Taylor column is present. Using a laser Doppler anemometer, axial and swirl velocity profiles are obtained at several stations upstream and downstream of the bubble, and in and around the bubble. The experimental velocity profiles, the stream surface plots, and the velocity distribution on the axis are compared with the corresponding results of solutions to the equation of inviscid rotating flow.

17. Key Words (Suggested by Author(s))	18. Distribution Statement
Vortex flows, breakdown, theoretical comparison, laser-doppler anemometer	Unclassified-Unlimited

19. Security Classif. (of this report)	20. Security Classif. (of this page)	21. No. of Pages	22. Price*
Unclassified	Unclassified	42	$3.00

*For sale by the National Technical Information Service, Springfield, Virginia 22151

ABSTRACT

Swirling flow in a rotating tube is studied by flow visualization at a moderate Reynolds number, and its velocity field is measured by laser-Doppler anemometry. The tube has constant diameter, and approximately uniform initial rigid rotation of the flow is assured by passing the flow through a rotating plug of porous metal before it enters the test section. At moderate swirl values, an object mounted on the tube centerline causes a closed bubble to form upstream of the obstacle, with a clearly defined stagnation point on the axis, and recirculating flow inside the bubble. The bubble length grows upstream as the swirl is increased, until it breaks up into a Taylor column reaching all the way upstream and downstream at swirl values above a certain critical value. A vortex jump (in the sense of Benjamin) occurs downstream of the obstacle except when the Taylor column is present. Using a laser Doppler anemometer, axial and swirl velocity profiles are obtained at several stations upstream and downstream of the bubble, and in and around the bubble. The experimental velocity profiles, the stream surface plots, and the velocity distribution on the axis are compared with the corresponding results of solutions to the equation of inviscid rotating flow.

I. INTRODUCTION

The problem under consideration is that of swirling flow (water, in this case) past an axisymmetric body of characteristic dimension a. The fluid and obstacle are contained within a cylindrical rotating tube of radius r_o. In its undisturbed state (no obstacle in the flow) the fluid is in rigid rotation with angular velocity Ω and has a uniform velocity w_o parallel to the axis of rotation except in the wall

boundary layer. In the presence of the obstacle a pronounced upstream effect is observed. We report here on flowfield measurements and the comparison with numerical results for the case where a stationary closed region of fluid containing recirculating flow is observed upstream of the obstacle. This region has a stagnation point at the upstream end; downstream it is closed by the obstacle itself. There is reversed axial flow near the axis. Two examples of the flow are shown in Plate 1. In view of its structure it seems appropriate to call the closed region a "vortex bubble". Whenever the vortex bubble is present, we have also observed downstream of the obstacle a rapid transition of the vortex flow to a different state. This "vortex jump" has all the features of the hydraulic jump analogy of Benjamin (1967). When the swirl ratio of the flow reaches a certain critical value, the vortex bubble and vortex jump disappear abruptly, and are replaced by a cylindrical column extending through the entire test section upstream and downstream of the obstacle. This critical value thus divides supercritical flow (vortex bubble) from subcritical flow (column).

The basic upstream effect was discovered experimentally by Taylor (1922). Using a sphere of radius $\underline{a}$ as the obstacle, he observed that for a Rossby number, $\epsilon = \frac{w_o}{a\Omega}$, less than about 0.32, a column of fluid, of the same diameter as the sphere was pushed along in front of the sphere as it moved along the axis of the rotating fluid. This column has since been called the "Taylor column"; it has also been studied by Long (1953), who has estimated that fluid is "pushed" ahead of the body only when ϵ is less than about 0.23. Pritchard (1969) has termed this effect

the "blocking" phenomenon, a situation in which fluid placed in front of the body is pushed ahead of it for all time.

Most theories (Morgan 1951, Stewartson 1952, Bretherton 1967) have considered these flows only when $\epsilon \ll 1$, ultimately yeilding a stagnant column of fluid extending far ahead of and behind the body. Studies at larger finite values of ϵ have been made by Stewartson (1968) and Lighthill (1967); their results have raised a question as to whether or not there is a maximum value of ϵ beyond which upstream influence cannot occur. Maxworthy (1970) has reported that a "forward wake" (as it has also been called by Stewartson (1970) is probably present for values of ϵ as large as 1.

Greenspan (1968) has conjectured that a column of fluid is trapped in front of the body (the blocking phenomenom) at all Rossby numbers less than about 0.7. He bases this assertion on his solution of the time-dependent flow of a disk that moves slowly along the axis of rotation after an impulsive start; in the flow ahead of the disk there is a stagnation point behind which exists a reversed cellular flow. Except for the prediction that the stagnation point advances upstream[1] with a velocity of $0.675\ a\Omega$, Greenspan's flowfield follows closely that predicted by Bossel (1967), and that reported herein.

The flowfield computations of Bossel (1967, 1969) gave closed bubbles of the type shown on Plate 1. However, for lack of experimental data these computations

---

[1]This advancement has also been predicted by Benjamin (1970).

were based on an assumed downstream axial velocity profile. In the present paper the same computational method is again applied using the measured downstream axial velocity profile, and computed and measured results over the whole flowfield are compared.

The vortex jump downstream of the obstacle has been previously observed, perhaps not quite as clearly as reported here. Long (1953) has reported the presence of a "strong, cyclonic" change in the vortex behavior behind a symmetrical obstacle moving along the axis of a rotating flow. Stewartson (1970), Pritchard (1969), and Maxworthy (1970) have considered this behavior to be a finite-transition in the sense of Benjamin (1967), since it appears as a "jump" from one state of flow to another. We present here a set of velocity measurements through the vortex jump region.

Miles (1972) has theoretically determined that forward separation should first occur for a disk at a critical Rossby number of $\epsilon = 1.05$, which is in good agreement with our observations. Miles also predicts steady-state reversed axial flows within the separation region and a forward stagnation point which only advances rapidly upstream for Rossby numbers smaller than 0.67, whereas our measurements indicate Taylor column formation for $\epsilon < 0.2$.

The measurement of a swirling flowfield requires some caution since the disturbance caused by an intrusive probe can be large enough to modify the flow and the data substantially. The laser Doppler velocimeter is a nonintrusive method of measurement and eliminates this complication. This technique has been successfully applied to the present problem. From the resulting data, stream surface plots are

determined by a simple integration. These plots, axial velocity profiles, and the velocity distribution along the axis are compared with the corresponding results from solutions to the equation of inviscid rotating flow.

II. EXPERIMENTAL APPARATUS

1. Rotating Flow System

A diagram of the rotating flow apparatus is shown in Figure 1. The rotating cylindrical plexiglass test section is 61 cm long with an inner diameter of 10.8 cm. It is a friction fit into aluminum housings which each contain a "shower-head" type fixture for dispersing the water as it enters and leaves the system. To give uniformity to the entrance flow, two slabs of General Electric porous nickel "Foametal" are inserted into the entrance housing; these porous plugs have an average pore size of 1.53 mm and are 2.5 mm thick. The entire unit rotates and is belt-driven by a 1/3-hp variable-speed motor. Mechanical rotating seals are used for sealing at the inlet and outlet.

The water system is "closed", and a flowmeter mounted downstream of the test section continuously monitored the flow rate which was found steady to ±1%. The rotation rate was monitored and found to be steady and reproducible.

Axisymmetric obstacles (sphere, disk, etc.) were mounted along the axis of the test section on a stainless steel rod. They remained stationary and did not rotate with the tube. Dye was injected through this rod into the flow at a position centered at the top of the obstacle in order to visualize the inner flow. Dye could also be injected at the entrance section to mark the outer flow.

2. Laser Doppler Anemometer

The concept of laser Doppler velocity measurement was first reported by Yeh and Cummins (1964). Since then it has been reported in many geometrical configurations, and each specific arrangement is usually a result of the requirements of the problem to which the anemometer is to be applied. The optical design chosen for this experiment and the associated electronics used for signal analysis are shown schematically in figure 2. Coherent laser light scattered from a fluid moving with velocity $\underline{v}$ is Doppler-shifted in frequency by an amount

$$\Delta\nu = \frac{n}{\lambda_o} \underline{v} \cdot (\underline{k}_s - k_i) \qquad (1)$$

where λ_o is the vacuum laser wavelength, and n is the index of refraction of the scattering medium; $\underline{k}_s$ and $\underline{k}_i$ are unit vectors in the directions of the scattered and incident waves, respectively. When the scattered and the incident (unshifted) waves are recombined at the photocathode of a photomultiplier tube, a beat signal is produced at frequency $\Delta\nu$ which is linearly related to the average velocity of the fluid within a small scattering volume (for this instrument about 0.20 mm^2 by 0.5 mm length).

The laser has an output power of 5 milliwatts. Even though it is of relatively low power, good heterodyning has been obtained by using a series of mirrors (figure 2) which allows forward-scattered light to be collected by the collecting lens; these mirrors form an attachment which is mounted to the front of the anemometer.

Figure 2 depicts the anemometer in the "swirl" velocity mode (as applied to vortex measurements). When the optical arm is rotated by 90° the anemometer is in the "axial" velocity mode. Refractions of the scattered beam at the water-plexiglass-air interfaces are accounted for by optical ray tracing; a set of correction equations are obtained which yield the true radial position within the test section. The instrument has continuous traversing capability by means of a fine-thread slide mechanism; reading accuracy of the slide scale is ±0.25 mm. The overall instrument resolution which could be obtained was ±0.5 mm.

In order to insure a high scattered-light intensity, polystyrene latex spheres of 0.5 micron diameter were added to the water; good heterodyne signals were obtained, and no further investigation was made to optimize the signal by varying the latex concentration and particle diameter.

Further details of this instrument are available in a report by Bossel and Orloff (1972).

III. EXPERIMENTAL RESULTS

1. Dye Studies

Plate 2 illustrates the type of flowfield under investigation. Dye has been injected from both upstream (at the entrance) and downstream (top of sphere). A retardation of the velocity along the axis was clearly observed, whereas at larger radii the flow quickly reached the obstacle. There is also a gradual expansion of the streamlines, with all of the upstream dye near the axis drawn into a very thin high velocity layer on the sphere before it passes around to the rear without

separation.[2] As the upstream fluid flows around the vortex bubble the two regions do not mix, indicating that the bubble is defined by a closed streamsurface with a stagnation point at the upstream end.

After moving over the downstream side of the sphere in a thin unseparated layer, the fluid leaves the sphere in a swirling laminar stream of small diameter. However, it quickly indergoes a jumplike turbulent transition to a much larger diameter, and proceeds downstream in a cylindrical swirling wake. This "vortex jump" follows Benjamin"s (1962, 1967) analogy to the hydraulic jump of open channel flows, which involves a finite transition between two distinct states of flow. More experimental evidence for this explanation is offered below.

Of interest is the behavior of the vortex bubble as the swirl changes. Figure 3a is a plot of bubble length against the inverse Rossby number $\alpha = \frac{a\Omega}{w_o}$. Data are given for the length of the bubble after a steady state has been reached for both increases and decreases in α. In the experiments, with their relatively low Reynolds numbers ($500 < Re_z < 1500$), hysteresis effects were apparent in the length of the bubble, but $Re_z \tilde{=} 1450$ was sufficiently high to minimize this effect, as demonstrated by the reversibility in figure 3a.

Below a value of $\alpha \tilde{=} 1.3$ no vortex bubble is observed. When the swirl is increased beyond a certain value, the bubble abruptly changes its structure and under-

---

[2]Since the axial Reynolds number Re_z is approximately 500, this flow without rotation would result in separation.

goes a transition to the well-known Taylor column at an inverse Rossby number of about 4.5. The first stages of this transition are seen as a breaking up of the vortex bubble, the enclosed dye moving out in sheets to form the outer boundary of the Taylor column. The column then proceeds rapidly upstream through the entrance porous metal and the flow becomes completely cylindrical with a diameter near that of the obstacle. In addtion, the vortex jump at the base of the sphere vanishes at this point and the upstream and downstream conditions become similar.

The inception of the bubble and the transition to a Taylor column were likewise found to be strongly Reynolds number dependent (Orloff 1971). At the lower Reynolds numbers the apparent convergence of the flow tube (and the associated pressure gradient) due to a greater thickening of the wall boundary layer caused both bubble and Taylor column formation to occur at higher swirl ratios for decreasing Re_z. Figure 3b shows the swirl ratios, $S = \frac{r_o \Omega}{w_o}$, required for transition at various Reynolds numbers. For very large Re_z the trend is toward asymptotic values of the swirl ratio which represent the absence of a wall boundary layer.[3] This same trend was found by Torrance and Kopecky (1971) in their viscous computations of axisymmetric vortex breakdowns in cylindrical streamtubes.

[3]The early experiments of Taylor (1922) and the more recent of Pritchard (1969) are for obstacles moving axially through a rotating cylindrical test section (in which no axial flow is present and hence no wall boundary layer exists) whose interior fluid is in initially rigid rotation.

Greenspan's prediction of reversed cellular flow for $\alpha \tilde{=} 1.5$ is strikingly close to the extrapolated value of 1.3 in figure 3a, which according to figure 3b should be near the inviscid limit. The exact value of α for transition to the Taylor column is difficult to determine, but it is near 4.5 as shown in figure 3a. This is in general agreement with Taylor's often-quoted value of $\alpha \sim \pi$, and Long's 1953 observation of 4.4.

2. Laser Doppler Measurements

The attainment of an undisturbed flow condition with w_o uniform and the flow in rigid rotation is complicated by the effect of a radial pressure gradient induced by the rotation,

$$\frac{\partial p}{\partial r} \simeq \rho \frac{v^2}{r}$$

which for rigid rotation is

$$\frac{\partial p}{\partial r} \simeq \rho \Omega^2 r \qquad (2)$$

A laser Doppler study was undertaken to determine if <u>any</u> state of approximately uniform flow and rigid rotation could be obtained in the experimental flow system. Figure 4a shows the manner in which the axial profile near the entrance[4] was

[4]A limitation of the experimental apparatus was that velocity profiles could not be obtained immediately downstream of the entrance porous metal; the closest profiles were obtained at approximately one tube radius, r_o, downstream.

influenced by rotation (for a constant flow rate) when no obstacle was present. The initial increase in velocity on the axis (with increasing Ω) is attributable to the radial pressure gradient of equation (2), but the cause for the subsequent decrease at higher values of Ω is not known. At any rate, for $\Omega = 3.48$/sec the flow was found to be reasonably uniform ($w_o \simeq 1.5$ cm/sec); the axial flow profiles at this rotation rate were measured and found nearly identical along the length of the test section (figure 4b). The swirl velocity profiles were also measured and found to be nearly that of rigid rotation for the length of the test section (figure 5).

Into this undisturbed flow condition was placed a disk (radius 1.27 cm) with a conical afterbody (1.27 cm long). The vortex bubble which resulted for $\Omega = 3.48$ sec^{-1} and $w_o \cong 1.5$ cm/sec is shown in Plate 3. This bubble was just below the critical length for transition to a Taylor column. The importance of this fact will become apparent later.

The flowfield both upstream and downstream of the disk surface was then quantitatively mapped with the laser velocimeter. The measured upstream axial and swirl velocity profiles are shown in figure 6. The retardation along the axis with eventual stagnation and subsequent reversed axial flow agrees with the flow visualization of Plate 2. In addition, a region of accelerated flow develops outside of the vortex bubble at about $r = 0.2\ r_o$ with velocities more than twice the free-stream velocity at the exit station (disk surface).

The swirl velocity profile remains nearly invariant with increasing z, except very near the disk surface where viscous effects predominate and the velocity must

vanish. This lack of response of the swirl profile to substantial variations in the axial profile is significant and has also been observed and reported by Chigier and Chervinsky (1967) in the measurement of swirling jets; it is also characteristic of Bossel's numerical solutions to the equations of inviscid swirling flows which will be discussed later in more detail.

Profiles measured downstream of the disk surface are given in figure 7. Upstream of the region where the vortex jump is observed to occur, the axial profile develops much as it did further upstream. The swirl velocity, however, shows a pronounced increase adjacent to the disk which is thought to develop as the fluid attempts to converse its angular momentum. Near the jump region, violent fluctuations in the laser Doppler velocity signal were indicative of highly unsteady, turbulent flow (shown by flow visualization in Plate 2). Further downstream the flow was observed to be steady, the accelerated flow region having lost part of its momentum in the turbulent vortex jump. Correspondingly, the increase in the swirl profile has vanished, and the swirl velocity profile has again become nearly linear.

The stream function for an axisymmetric flow is related to the axial velocity component by

$$w = \frac{1}{r}\frac{\partial \psi}{\partial r} \quad .$$

The experimental axial velocity profiles of figures 6 and 7 were therefore integrated numerically to obtain the streamline plot shown in figure 8.

ψ^* is a nondimensional stream function

$$\psi^* = \psi(r) / \psi_{ENT}(r_o)$$

where $$\psi(r) = \int_o^r wr\, dr$$

and $$\psi_{ENT}(r_o) = \frac{1}{2} w_o r_o^2$$

The accelerated flow region (converging streamlines) and the vortex jump are both apparent. Furthermore, one observes that the flow upstream of the obstacle remains cylindrical for $r/r_o > .36$, indicating a "core" region within which the dynamics of the upstream influence are contained.

The velocity on the axis was measured and is plotted in figure 9 as a function of swirl for rotation rates between zero and 3.48/sec. The effect of the radial pressure gradient (equation (2)) is clearly evident when the data are extrapolated to the entrance (the same trend can be seen in figure 4a). It is clear that the upstream effect becomes more important as rotation increases, until for $\Omega = 3.48$/sec the decrease in axial velocity is nearly linear; for $\Omega > 3.48$/sec no curve exists due to Taylor column formation. Extrapolation of this linear profile to the entrance suggests a characteristic freestream velocity of $w_o \sim 0.9$ cm/sec. This does not agree with figure 4b which yielded $w_o \tilde{=} 1.5$ cm/sec. This discrepancy may indicate that the flow exactly at the entrance is not uniform, but has been influenced by the obstacle, its presence sensed upstream through the porous metal. The other possibility is that the curve does not continue linearly to $z = 0.0$.

If the data for the incipient bubble are extrapolated to the axis, w_{ax} ($z = 0$) = 2.3 cm/sec. Using $\Omega = 1.74$/sec and a disk radius of 1.27 cm one calculates a critical Rossby number of $\epsilon_* = \frac{w_o}{a\Omega} = 1.04$, in agreement with Miles (1972) prediction of 1.05.

IV. COMPARISON WITH COMPUTATIONAL RESULTS

The basic equation describing incompressible, inviscid, steady, rotating axisymmetric flow in a Newtonian frame can be written in cylindrical coordinates (r, θ, z) as

$$\frac{\partial^2\psi}{\partial r^2} - \frac{1}{r}\frac{\partial\psi}{\partial r} + \frac{\partial^2\psi}{\partial z^2} = -k\frac{dk}{d\psi} + \frac{r^2}{\rho}\frac{dp_o}{d\psi} \tag{3}$$

(for example, see Batchelor 1967) where ψ is the streamfunction chosen to satisfy continuity; $k(\psi) = rv$ is the circulation function, and $p_o(\psi) = p + \frac{\rho}{2}(u^2 + v^2 + w^2)$ represents the total pressure; $u = \frac{-1}{r}\frac{\partial\psi}{\partial z}$ is the radial velocity, $w = \frac{1}{r}\frac{\partial\psi}{\partial r}$ is the axial velocity.

Considering the order of magnitude of each term in the Navier-Stokes equation, Bossel (1967, 1969) has determined that equation (3) should be applicable within the central portion of a vortex which closely approximates rigid rotation. This core is what the apparatus described earlier was intended to simulate.

The condition of initial rigid rotation Ω and uniform axial flow w_o linearizes equation (3). Introducing the following set of nondimensional variables,

$$R = \frac{r}{r_c} \qquad U = \frac{u}{w_o} \qquad \Psi = \frac{\psi}{w_o r_c^2}$$

$$Z = \frac{z}{r_c} \qquad V = \frac{v}{w_o} \qquad K = \frac{vr}{w_o r_c} \tag{4}$$

$$W = \frac{w}{w_o} \qquad P = \frac{p}{\rho w_o^2}$$

one obtains

$$\frac{\partial^2\Psi}{\partial Z^2} - \frac{1}{R}\frac{\partial\Psi}{\partial R} + \frac{\partial^2\Psi}{\partial R^2} = -4\left(\frac{r_c\Omega}{w_o}\right)^2 \Psi + 2\left(\frac{r_c\Omega}{w_o}\right)^2 R^2 \tag{5}$$

or, introducing the swirl parameter $\Gamma = \frac{r_c\Omega}{w_o}$,

$$\frac{\partial^2\Psi}{\partial Z^2} - \frac{1}{R}\frac{\partial\Psi}{\partial R} + \frac{\partial^2\Psi}{\partial R^2} = -4\Gamma^2\Psi + 2\Gamma^2 R^2 \tag{6}$$

The general solution to equation (6) has been obtained by Long (1953). Applying the following boundary conditions[5] to Long's solution,

[5] We note that equation (6) is elliptic and requires specification of the complete boundary enclosing the region of interest. However, Bossel points out that specification of the pressure on the axis may be used as an alternative to specifying Ψ_L.

$\Psi(R,0) = \Psi_o = \frac{R^2}{2}$	rigid-body rotation at the entrance with uniform axial flow; $\psi_{ENT} = \frac{1}{2} w_o r^2$	(7)
$\Psi(0,Z) = 0$	the central streamline and the contour of the bubble are given by $\psi = 0$	(7)
$\Psi(1,Z) = \frac{1}{2}$	The outer surface of the vortex core is cylindrical with $\psi = 1$ at $r = r_c$ [6]	(7)
$\Psi(R,L) = \Psi_L(R)$	exit stream function	(7)

Bossel (1967, 1969) obtains

$$\Psi(R,Z) = \frac{R^2}{2} + R \sum_{o}^{\infty} C_n J_1 (j_{1n} R) \sinh \left\{ Z \sqrt{j_{1n}^2 - (2\Gamma)^2} \right\} \qquad (8)$$

[6] Since the only requirement for the specification of the core radius is that the outer streamline remain parallel, a core radius $r_c = 0.36\, r_o$ is chosen from figure 8. Discussions of an obstacle of dimension $\underline{a}$ in an unbounded flow ($r_c \to \infty$) lead to a description in terms of the Rossby number, ϵ, and its inverse, α. In the numerical approach of this section the obstacle size is inherent in the specification of the exit axial velocity profile, and the swirl parameter, Γ, is the quantity of interest.

where the j_{1n} are the zeros of the Bessel function J_1.

The C_n are Fourier-Bessel coefficients which may be determined, if Ψ_L is known, by

$$C_n = 2 \int_0^1 f(R)\, RJ_1 (j_{1n}R)\, dR/J_o^2 (j_{1n}) \sinh \left\{ L\sqrt{j_{1n}^2-(2\Gamma)^2} \right\} \quad (9)$$

with

$$f(R) = \frac{1}{R} \left[\Psi_L(R) - \frac{R^2}{2} \right]$$

The implication of the above solution is that if we can supply Γ and $\Psi_L(R)$ from experimental results, then, in principle, the interior flow can be obtained exactly with the infinite sum in equation (8), and to a close approximation by using only a finite number of terms. Bossel (1967) has determined that this solution converges rapidly with increasing n and that the inclusion of terms beyond n = 10 will not significantly change $\Psi(R, Z)$.

An important feature of the solutions is that for an increasing swirl parameter, $\Gamma = \frac{r_c \Omega}{w_o}$, the vortex bubble increases in length until, for any value greater than 1.91585, the solution becomes subcritical with infinite upstream influence. This is taken to represent the transition to a Taylor column.

As noted in section III. 1., the transition to a Taylor column occured for a value greater than 1.91585 due to the apparent convergence of the flow tube. Nevertheless, a valid comparison of experiment and inviscid solutions should be possible if both are set at the point of incipient transition to the Taylor column. This is done in the following comparison.

$\Psi_L(R)$ is generated by a Fourier-Bessel reproduction of the measured exit axial velocity profile according to equation (9). The reproduction is given as w/w_o vs. r/r_c; w_o is a value which allows the computational scheme to satisfy continuity. r_c and L are inputs which set the scale for the computational scheme.

The inviscid calculations predict that the swirl velocity should reverse sign within the vortex bubble. This is definitely not observed - the rotation always remains in the same sense; therefore no comparison of the swirl profiles can be made with experiment. It is felt, however, that since the axial and swirl velocity profiles remain highly uncoupled, it is the presence of the rotation and not its detailed structure that dominates the development of the axial velocity profile; a comparison of the experimental and calculated axial profiles should therefore be meaningful.

Axial velocity computations are shown in figure 10. Matching the exit profile to the computed values required that $w_o = 1.3$ cm/sec; this is higher than that indicated by figure 9, but smaller than that suggested in figure 4b. The profiles match extremely well in the vortex bubble region especially inside of the bubble where the predicted reversed axial flow agrees well with the measurements.

The predicted streamline plot is shown in figure 11. The predicted vortex bubble is exactly the same length and shape as that observed. In particular, very near the disk the bubble expands out quickly over a very small axial distance (less than a/10) to match the disk diameter. This is also observed experimentally as shown in Plate 3. It is for this reason that the measured profiles of figures 6, 7, and 10 indicate that an axial velocity exists at the outer portion of the disk, for it was not possible to make the laser Doppler measurements exactly at the surface of the disk.

The numerical scheme can be used for swirl parameters less than 1.91585, but one must have data for $\Psi_L(R)$. Lacking this data, the exit profile given earlier was used as the input for several different swirl values. In figure 12 the velocity on the axis is plotted versus downstream distance. Even though $\Psi_L(R)$ may not be correct, the similarity to figure 9 is striking. Again, as maximum swirl is approached, the curve becomes linear.

SUMMARY AND CONCLUSIONS

Laser Doppler anemometry has been successfully applied to the study of a swirling flow with upstream influence and recirculation. The flowfield which has been nonintrusively measured and reported appears not to have been previously well-documented except in the limit of Taylor column formation. We have in particular studied flows with confined recirculating flow regions (vortex bubbles) upstream of an obstacle, and the vortex jump occurring downstream of the obstacle.

Our experimental observations and the inviscid compuations suggest that the vortex bubble starts at the obstacle at a certain nonzero swirl value. It then grows in length with increasing swirl ratio until, at a certain critical swirl ratio, it is abruptly replaced by a Taylor column which reaches all the way upstream and downstream of the obstacle. The vortex bubble flow is supercritical upstream of the obstacle, while the columnar flow is subcritical. The swirl values for inception of the bubble and the critical swirl value dividing bubble from column flow are dependent on Reynolds number - lower Reynolds numbers having higher critical swirl values.

The measured vortex bubble flowfield has been compared with the computed bubble flowfield. The computational method uses the equation of inviscid rotating flow with initial rigid rotation. In both cases (experimental and computational) the swirl ratio was that of impending transition from the bubble to the Taylor column (supercritical to subcritical). The agreement of bubble shape, axial velocity profiles, and development of velocity on the axis is very good, leading to the conclusion that the inviscid dynamics almost entirely determine the overall features of the vortex bubble flowfield.

Flow visualization and velocity measurements downstream of the obstacle show the existence of a vortex jump if the upstream flow is supercritical. The inner streamsurfaces undergo a very rapid expansion at the location of the jump, which is also marked by strong turbulence. Through the jump, axial momentum is lost in the inner region. Downstream of the jump the inner flow continues as a cylindrical (subcritical) column.

The present experiments have dealt with "forced" vortex bubbles caused by the presence of an obstacle. We have also generated, but not yet measured, "free" vortex bubbles by appropriate shaping of the external stream surface (expansion and subsequent contraction) without the presence of an obstacle. Free vortex bubbles appear approximately at the same swirl parameter as forced bubbles and appear to be the same physical phenomenon. This is underscored by the fact that they can also be generated by the same computational procedure used to compute the forced vortex bubbles.

REFERENCES

Batchelor, G.K. (1967), An Introduction to Fluid Dynamics, Cambridge University Press.

Benjamin, T. B. (1962), "Theory of the vortex breakdown phenomenon," J. Fluid Mech. 14, 593-629.

Benjamin, T. B. (1967), "Some developments in the theory of vortex breakdown," J. Fluid Mech. 28, 65-84.

Benjamin, T. B. (1970), "Upstream influence," J. Fluid Mech. 40, 49-79.

Bossel, H.H. (1967), "Inviscid and viscous models of the vortex breakdown phenomenon," Ph. D. thesis, Univ. of Calif., Berkeley.

Bossel, H.H. (1969), "Vortex breakdown flowfield," Phys. Fluids 12, 498-508.

Bossel, H.H., and Orloff, K. L. (1972), "Laser-Doppler anemometer for water tunnel applications," J. Hydronautics 6, No. 2, July 1972.

Bretherton, F. P. (1967), "The time-dependent motion due to a cylinder moving in an unbounded rotating or stratified fluid," J. Fluid Mech. 28, 545-570.

Chigier, N.A., and Chervinsky, A. (1967), "Experimental investigation of swirling vortex motion in jets," ASME Transactions, J. Applied Mech. 34, 2, 443-451.

Greenspan, H.P. (1968), The Theory of Rotating Fluids, Cambridge University Press.

Lighthill, M.J. (1967), "On waves generated in dispersive systems by travelling forcing effects, with applications to the dynamics of rotating fluids," J. Fluid Mech. 27, 725-752.

Long, R.R. (1953), "Steady motion around a symmetrical obstacle moving along the axis of a rotating fluid," J. Meteorol. 10, 197-203.

Maxworthy, T. (1970), "The flow created by a sphere moving along the axis of a rotating, slightly-viscous fluid," J. Fluid Mech. 40, 453-479.

Miles, J.W. (1972), "Axisymmetric rotating flow past a circular disk," J. Fluid Mech. 00, 000-000.

Morgan, G.W. (1951), "A study of motions in a rotating liquid," Proc. Roy. Soc. Lond. A206, 108-130.

Orloff, K.L. (1971), "Experimental investigation of upstream influence in a rotating flowfield," Ph.D. thesis, Univ. of Calif, Santa Barbara. (available through University Microfilms, Ann Arbor, Michigan).

Pritchard, W.G. (1969), "The motion generated by a body moving along the axis of a uniformly rotating fluid," J. Fluid Mech. 39, 443-464.

Stewartson, K. (1952), "On the slow motion of a sphere along the axis of a rotating fluid," Proc. Comb. Phil. Soc. 48, 168-177.

Stewartson, K. (1968), "On inviscid flow of a rotating fluid past an axially-symmetric body using Oseen's equations," Quart. Journ. Mech. and Applied Math. 21, 353-373.

Stewartson, K. (1970), "A note on forward wakes in rotating fluids," J. Fluid Mech. 42, 219-223.

Taylor, G.I. (1922), "The motion of a sphere in a rotating liquid," Proc. Roy. Soc. Lond. 102A, 180.

Torrance, K. E., and Kopecky, R. M. (1971), "Numerical study of axisymmetric vortex breakdowns," NASA CR-1865.

Yeh, Y., and Cummins, H. Z. (1964), "Localized fluid flow measurements with an He-Ne laser spectrometer," Appl. Physics Letters 4, 176-178.

LIST OF PLATE CAPTIONS

Plate 1 - Vortex bubbles, showing upstream stagnation point and recirculating contained flow upstream of (a) a disk (4.30 cm dia) with a conical afterbody (b) a sphere (3.85 cm dia).

Plate 2 - Vortex bubble ahead of sphere (2.54 cm dia). Dye injected at top of sphere is contained within the vortex bubble. Dye injected upstream at the entrance flows around the bubble, through thin layer at the rear of the obstacle, then is ejected in a vortex jump.

Plate 3 - Vortex bubble ahead of disk (2.54 cm dia). Measurements of this flow structure are used for comparison with the numerical solutions. The bubble is near transition to the Taylor column; $w_o = 1.5$ cm/sec; $\Omega = 3.48$/sec.

LIST OF FIGURE CAPTIONS

Figure 1 - Rotating flow system.

Figure 2 - Optical layout and signal processing electronics for local oscillator laser-Doppler system.

Figure 3 - (a) Length of vortex bubble nondimensionalized by sphere radius, $a = 1.27$ cm, versus inverse Rossby number, α; $Re_z = \frac{r_o w_o}{\nu} = 1450$; $w_o = 2.9$ cm/sec.

(b) Swirl ratios $S = \frac{r_o \Omega}{w_o} = \alpha \frac{r_o}{a}$, required for transition at various Reynolds numbers, Re_z, showing asymptotic approach to inviscid values of S as $Re_z \to \infty$. Obstacle is a sphere of radius $a = 1.27$ cm.

Figure 4 - Undisturbed flow conditions (no obstacle)

(a) Variation of axial velocity profile with rotation

(b) Uniformity of axial velocity profile along the test section.

Figure 5 - Undisturbed flow conditions - swirl velocity profile for $w_o = 1.5$ cm/sec.

Figure 6 - Velocity measurements; upstream. Measurements of reversed axial flows are shown within vortex bubble. Disk diameter is 1.27 cm.

Figure 7 - Velocity measurements; downstream.

Figure 8 - Streamline plot constructed from axial velocity measurements of figures 6 and 7.

Figure 9 - Measured velocity on the axis versus distance downstream.

Figure 10 - Computed axial velocity profiles within computational region, based on Fourier-Bessel reproduction of exit velocity profile. —— theory; — — — experiment; w_o = 1.3 cm/sec.

Figure 11 - Streamline plot (theory) showing agreement in length and shape of observed vortex bubble.

Figure 12 - Computed velocity on the axis for various swirl parameters and a fixed exit profile.

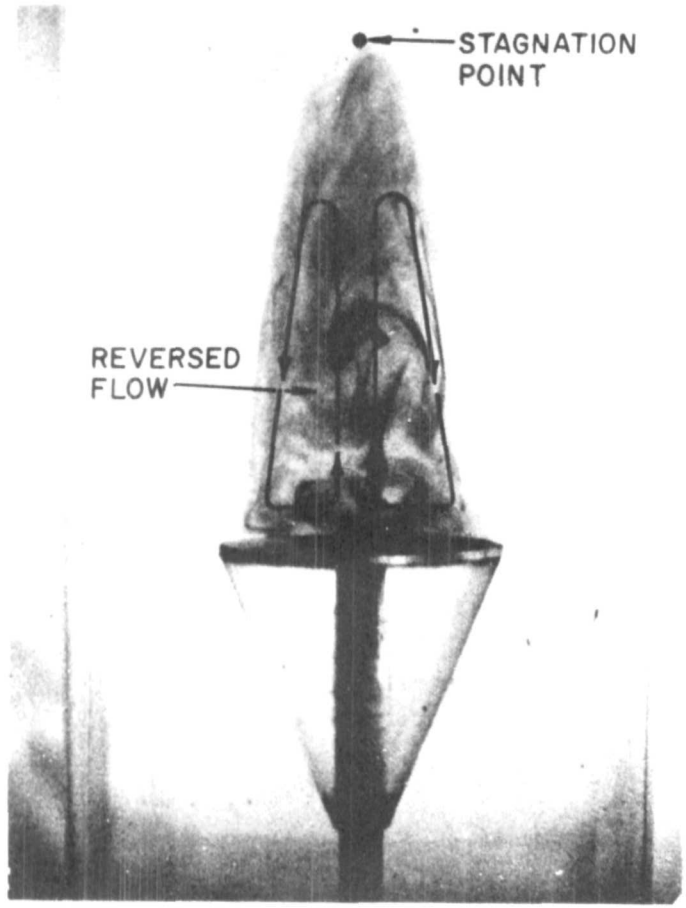

(a)

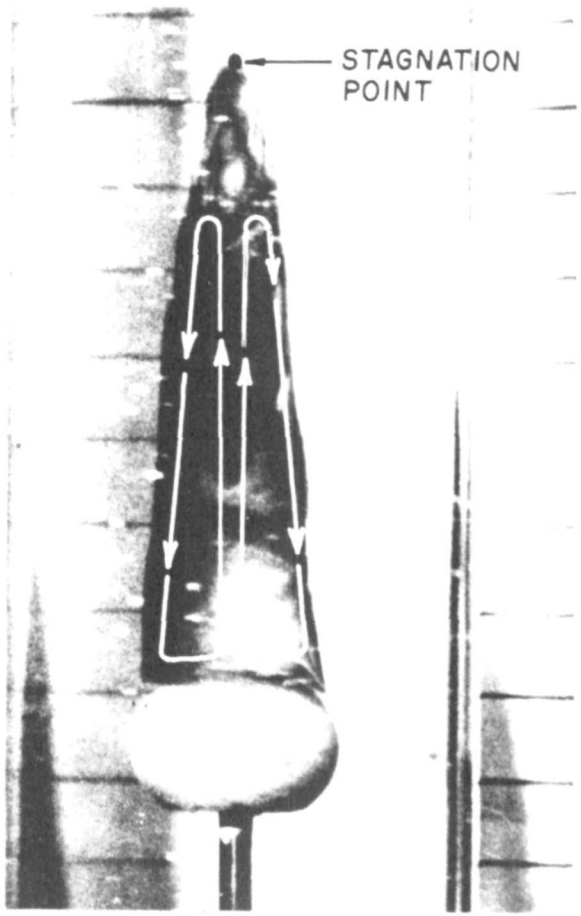

(b)

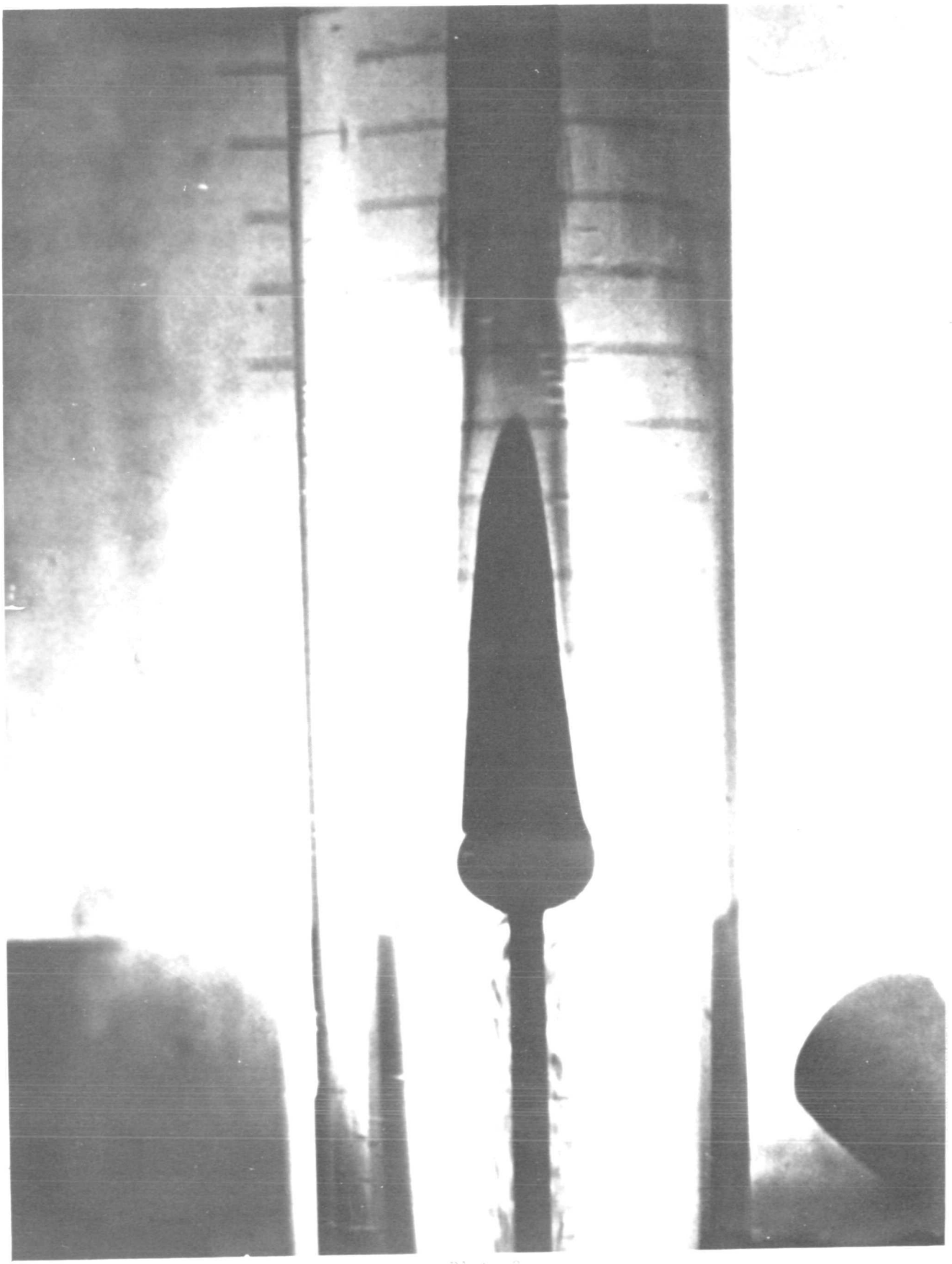

Plate 2

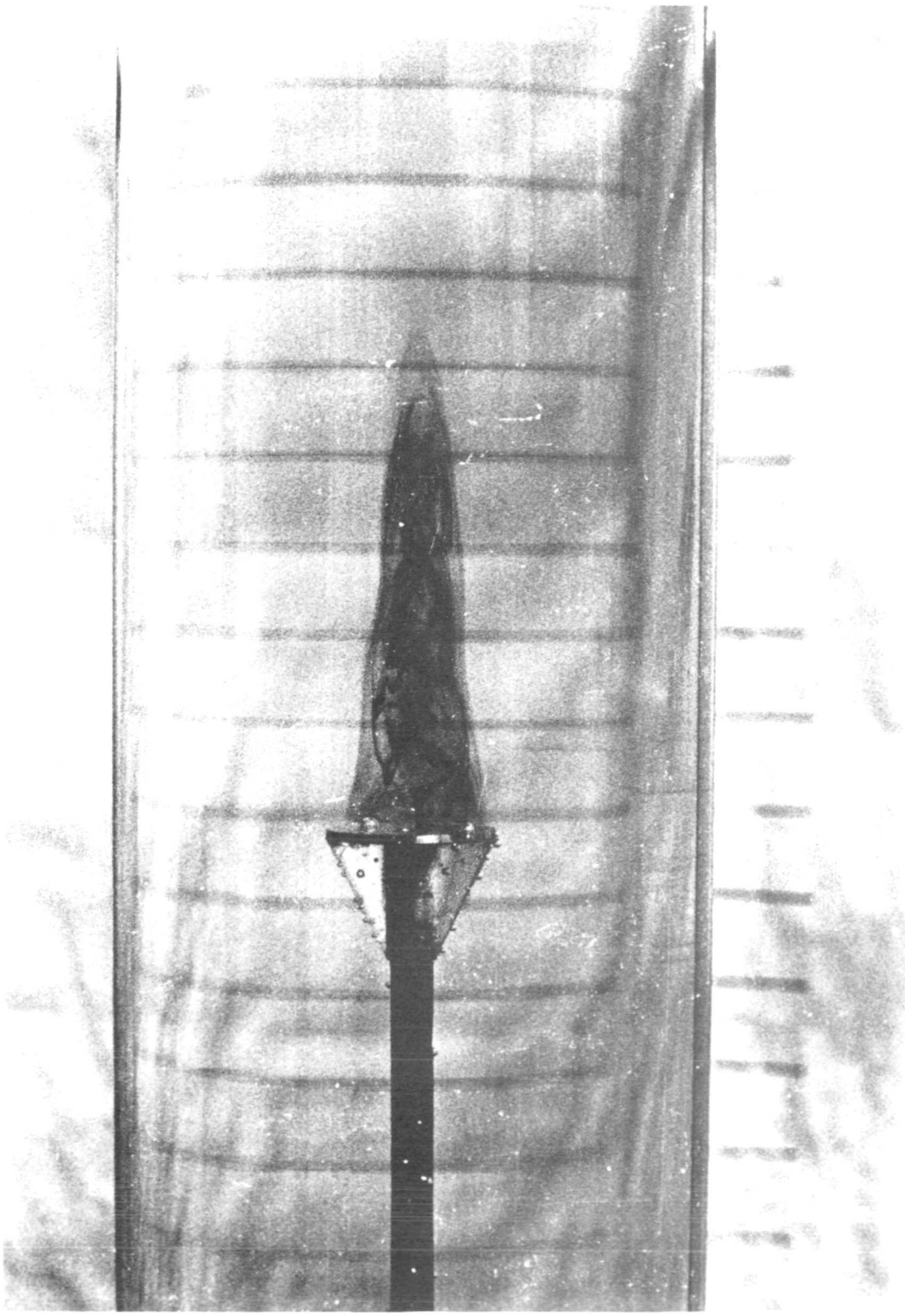

Plate 3

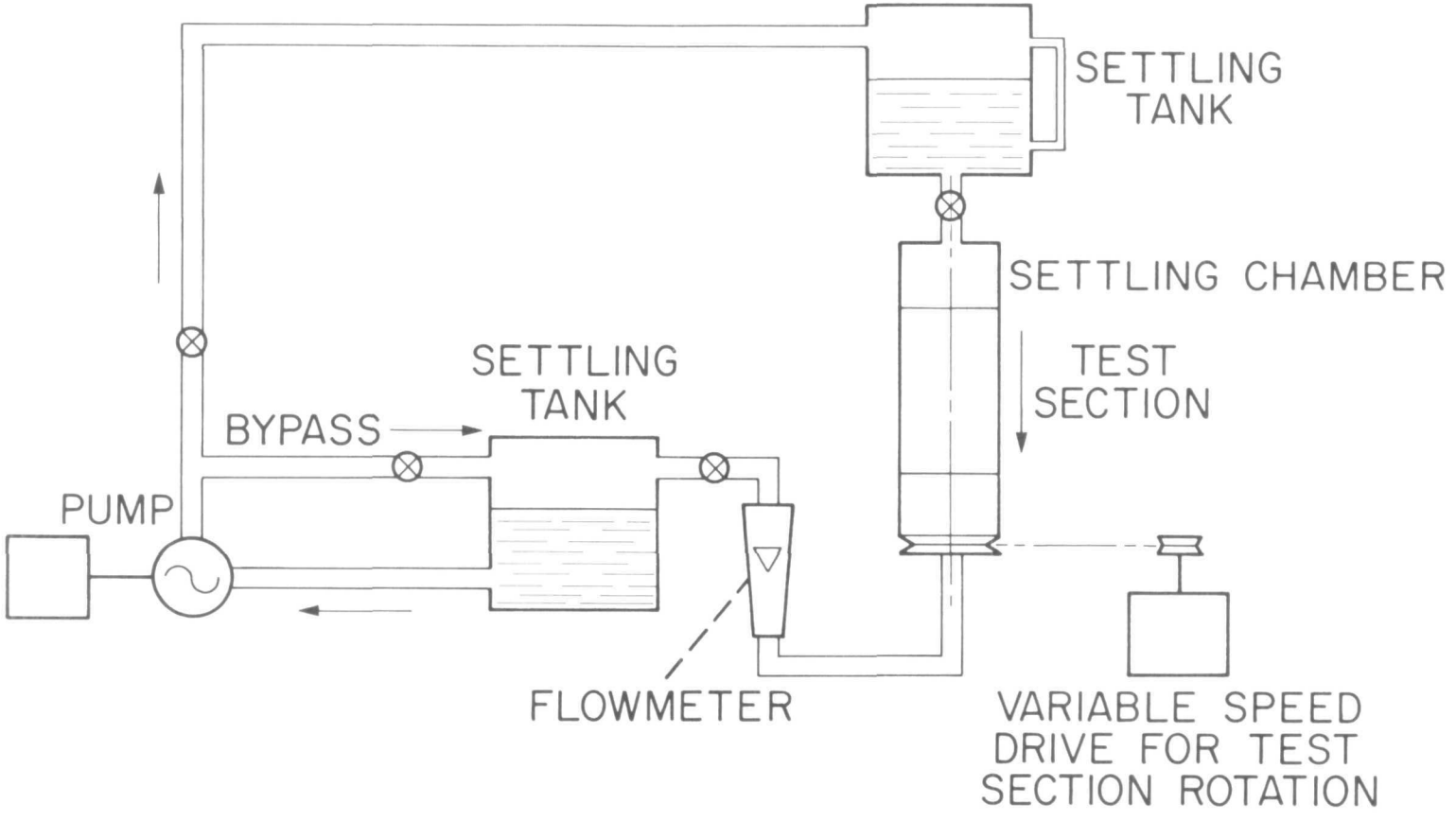
SETTLING
TANK
SETTLING CHAMBER
TEST
SECTION
SETTLING
TANK
BYPASS
PUMP
FLOWMETER
VARIABLE SPEED
DRIVE FOR TEST
SECTION ROTATION

Fig. 1

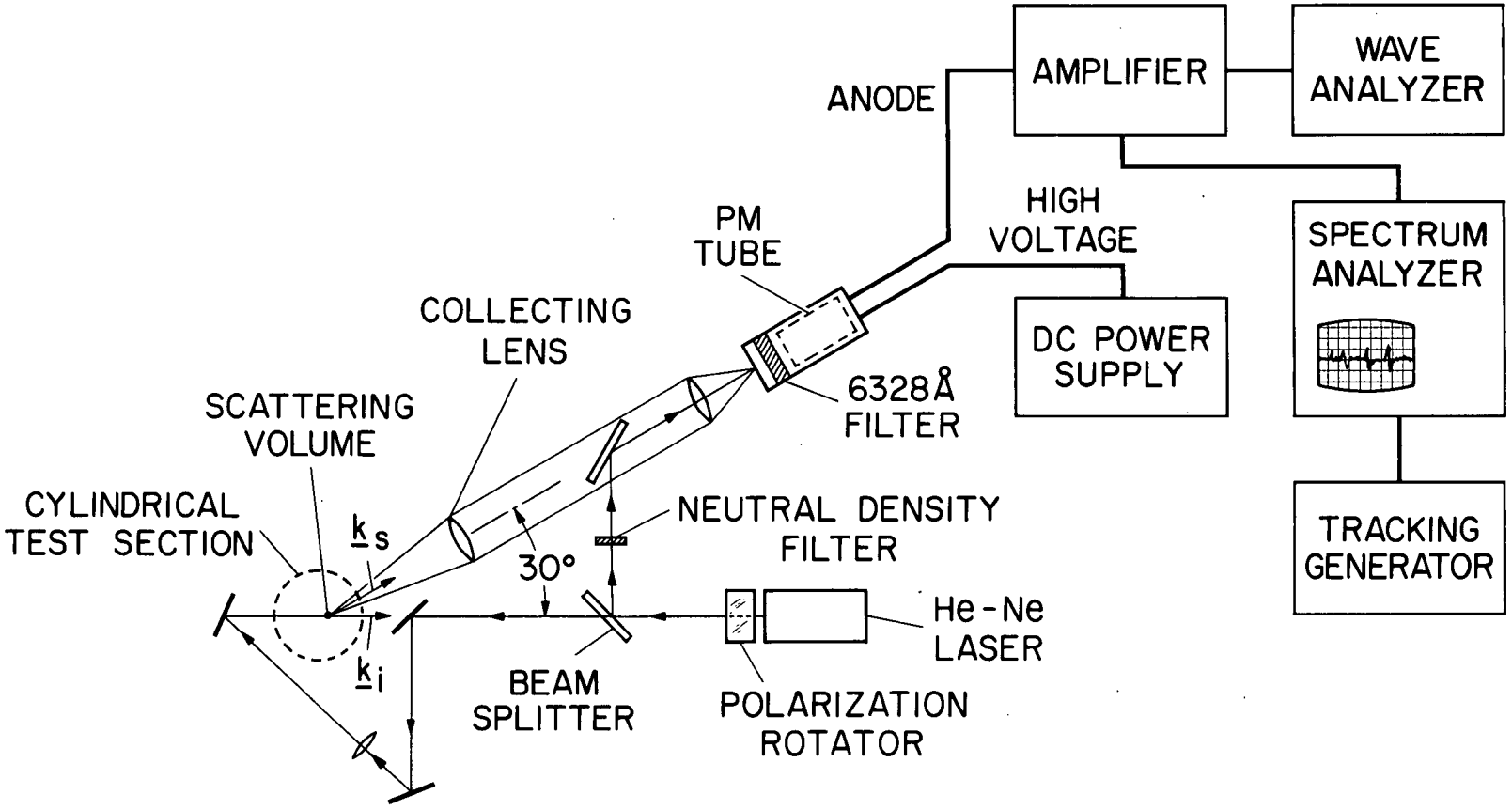
AMPLIFIER
WAVE ANALYZER
ANODE
HIGH VOLTAGE
PM TUBE
SPECTRUM ANALYZER
COLLECTING LENS
DC POWER SUPPLY
6328Å FILTER
SCATTERING VOLUME
CYLINDRICAL TEST SECTION
NEUTRAL DENSITY FILTER
TRACKING GENERATOR
30°
He-Ne LASER
BEAM SPLITTER
POLARIZATION ROTATOR

Fig. 2

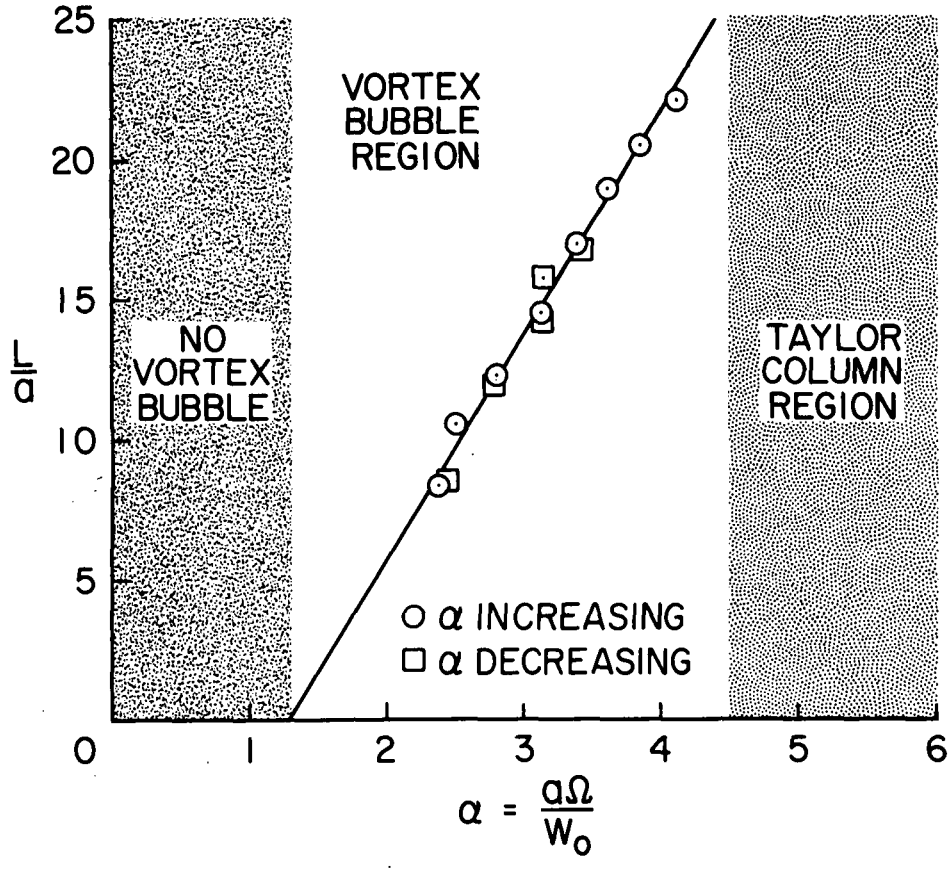
25
20
15
10
5
0
1
2
3
4
5
6
a_T
VORTEX
BUBBLE
REGION
NO
VORTEX
BUBBLE
TAYLOR
COLUMN
REGION
○ α INCREASING
□ α DECREASING
$\alpha = \frac{a\Omega}{W_o}$

Fig. 3(a)

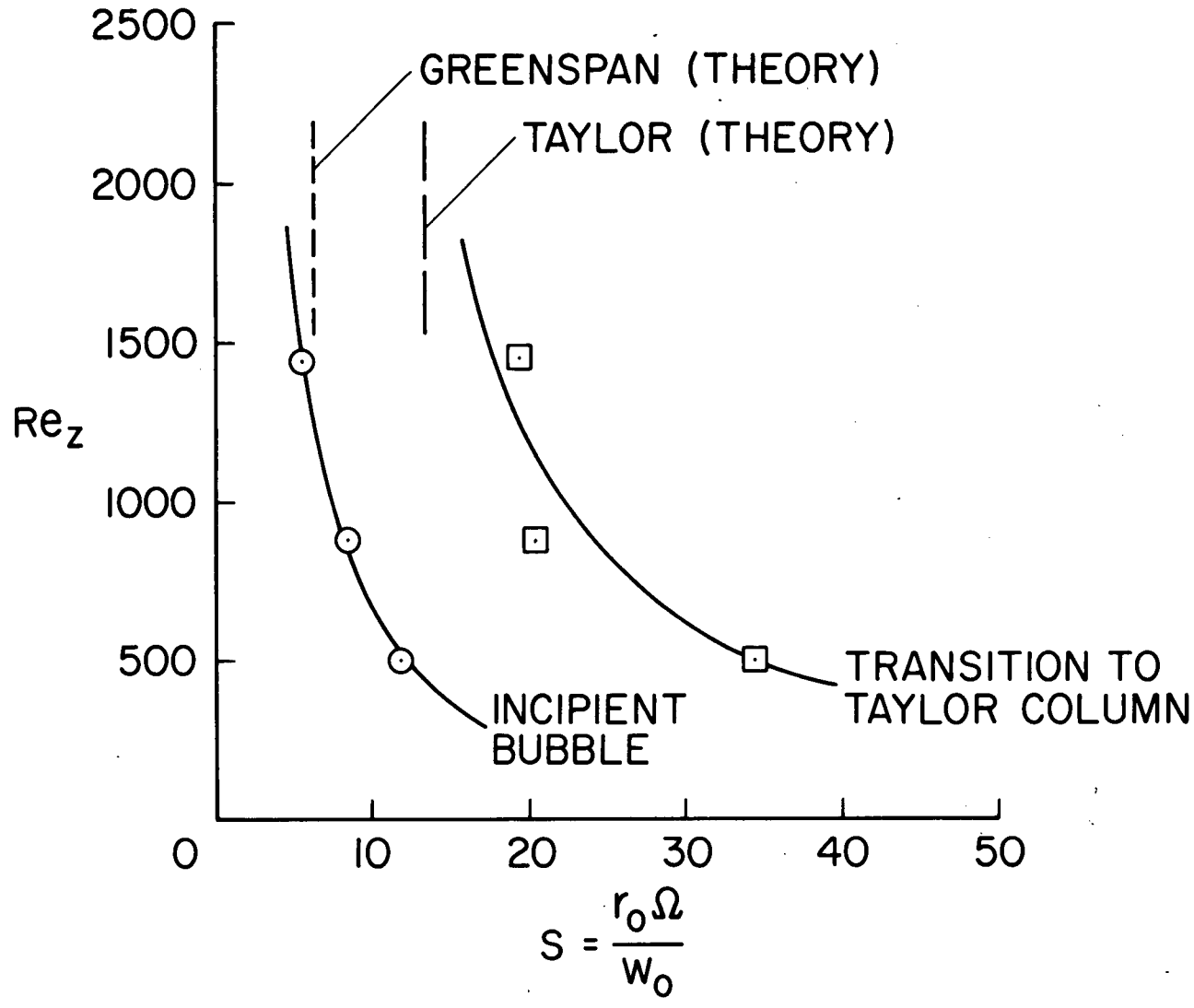
2500
2000
1500
1000
500
0
10
20
30
40
50
Re_z
GREENSPAN (THEORY)
TAYLOR (THEORY)
INCIPIENT BUBBLE
TRANSITION TO TAYLOR COLUMN
$S = \frac{r_0 \Omega}{w_0}$

Fig. 3(b)

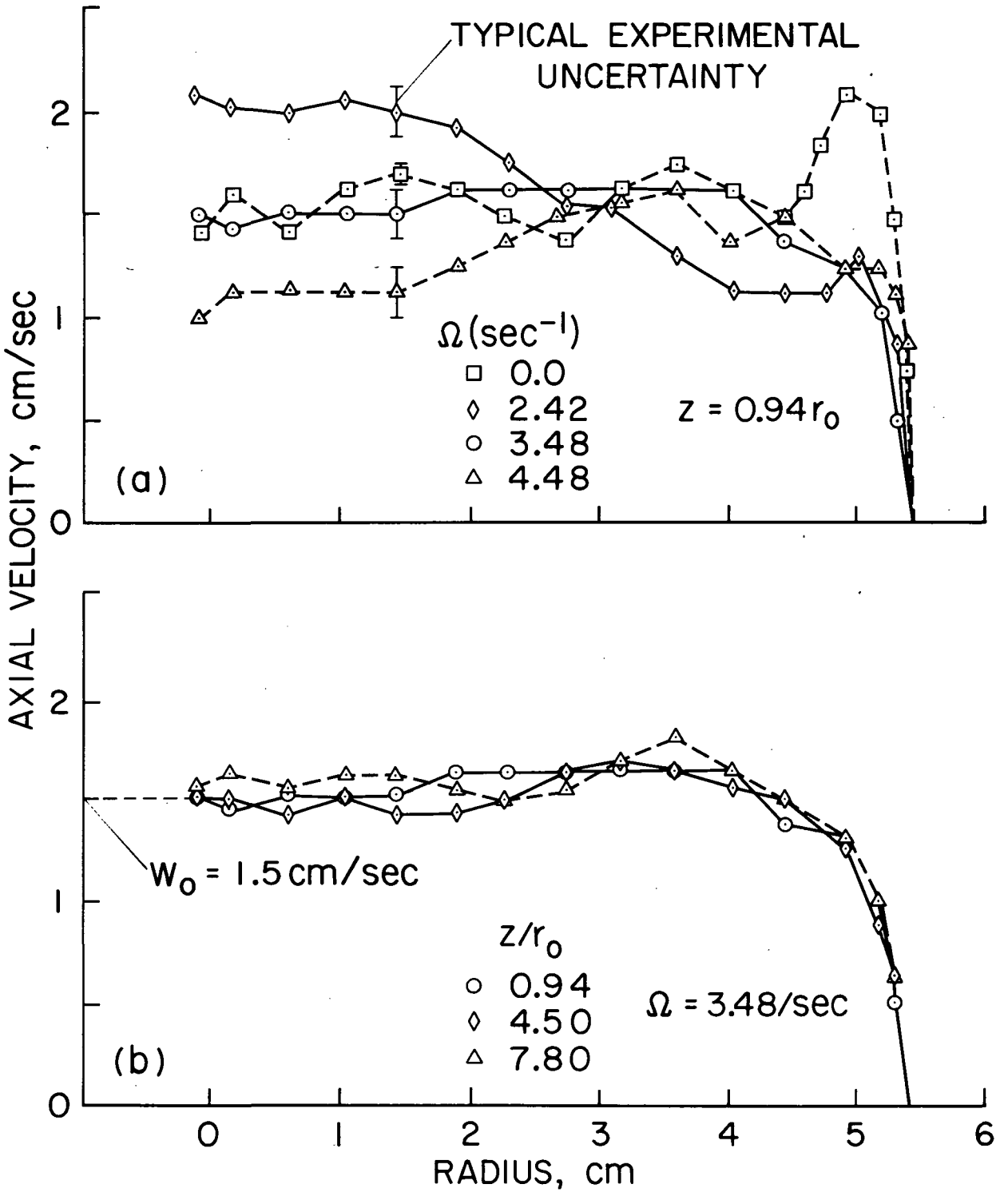
TYPICAL EXPERIMENTAL
UNCERTAINTY
Ω(sec⁻¹)
0.0
2.42
3.48
4.48
z = 0.94r₀
(a)
AXIAL VELOCITY, cm/sec
W₀ = 1.5 cm/sec
z/r₀
0.94
4.50
7.80
Ω = 3.48/sec
(b)
RADIUS, cm

Fig. 4

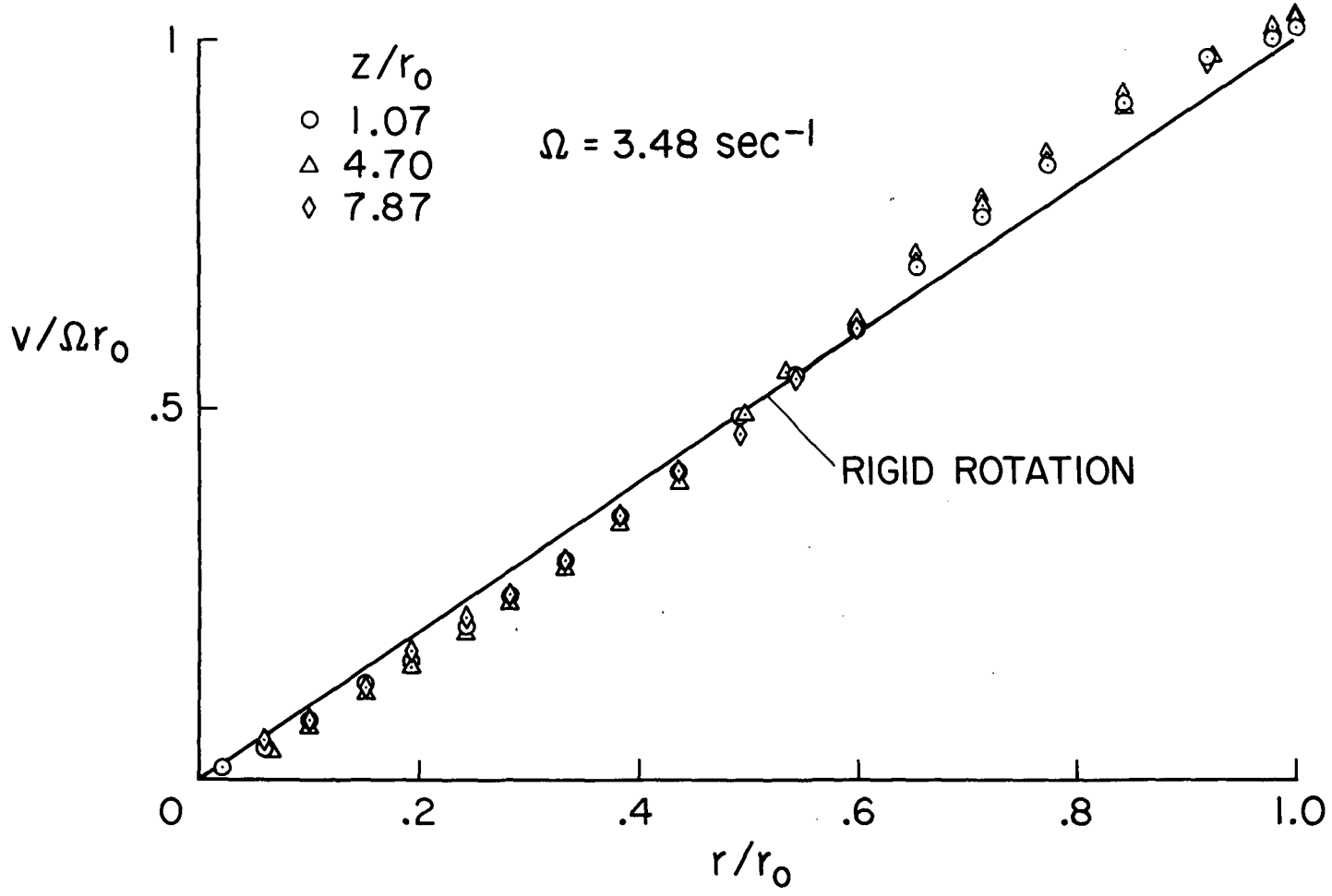

Fig. 5

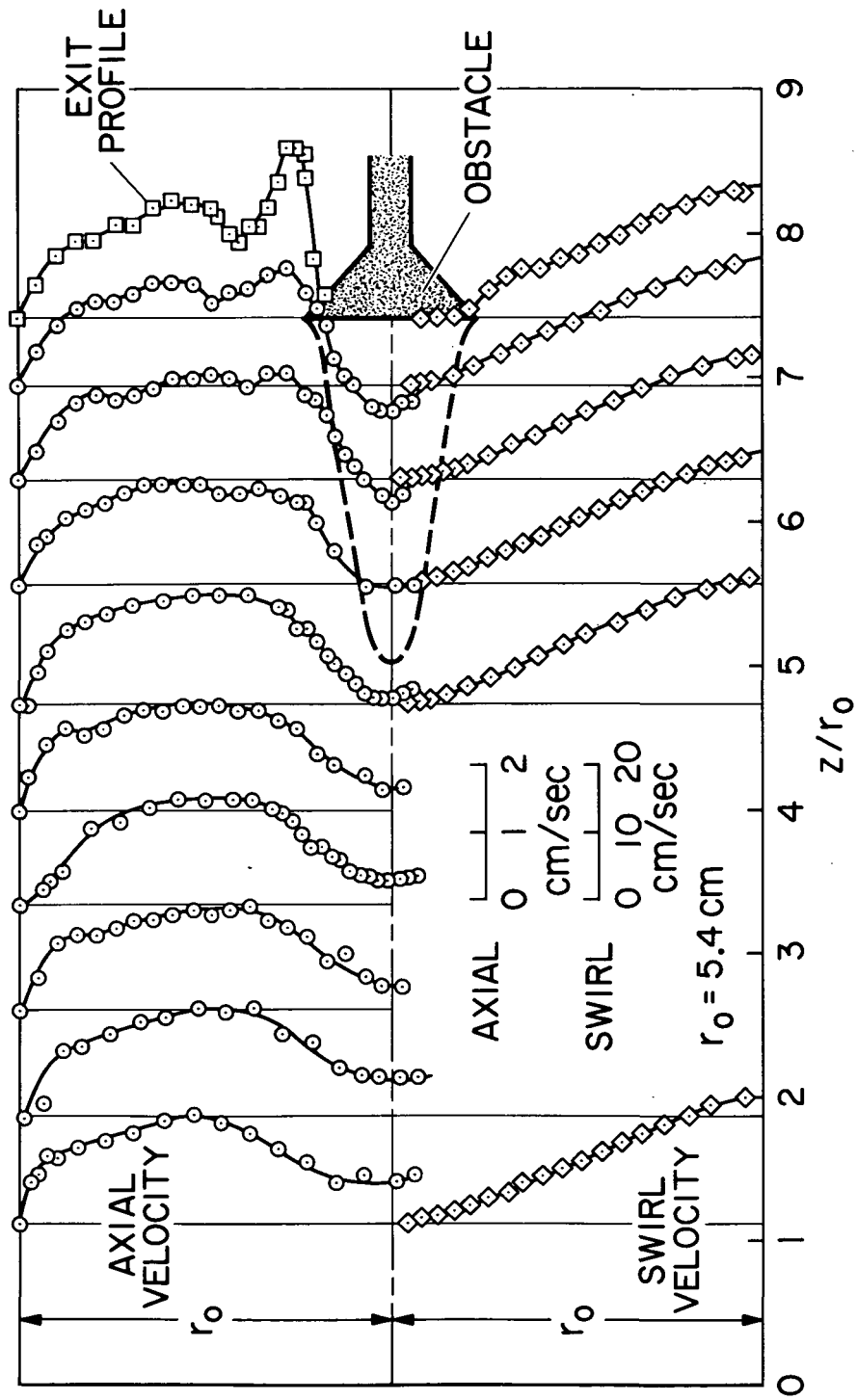
EXIT PROFILE
OBSTACLE
AXIAL VELOCITY
SWIRL VELOCITY
r_o
r_o
AXIAL 0 1 2 cm/sec
SWIRL 0 10 20 cm/sec
r_o = 5.4 cm
0 1 2 3 4 5 6 7 8 9
z/r_o

Fig. 6

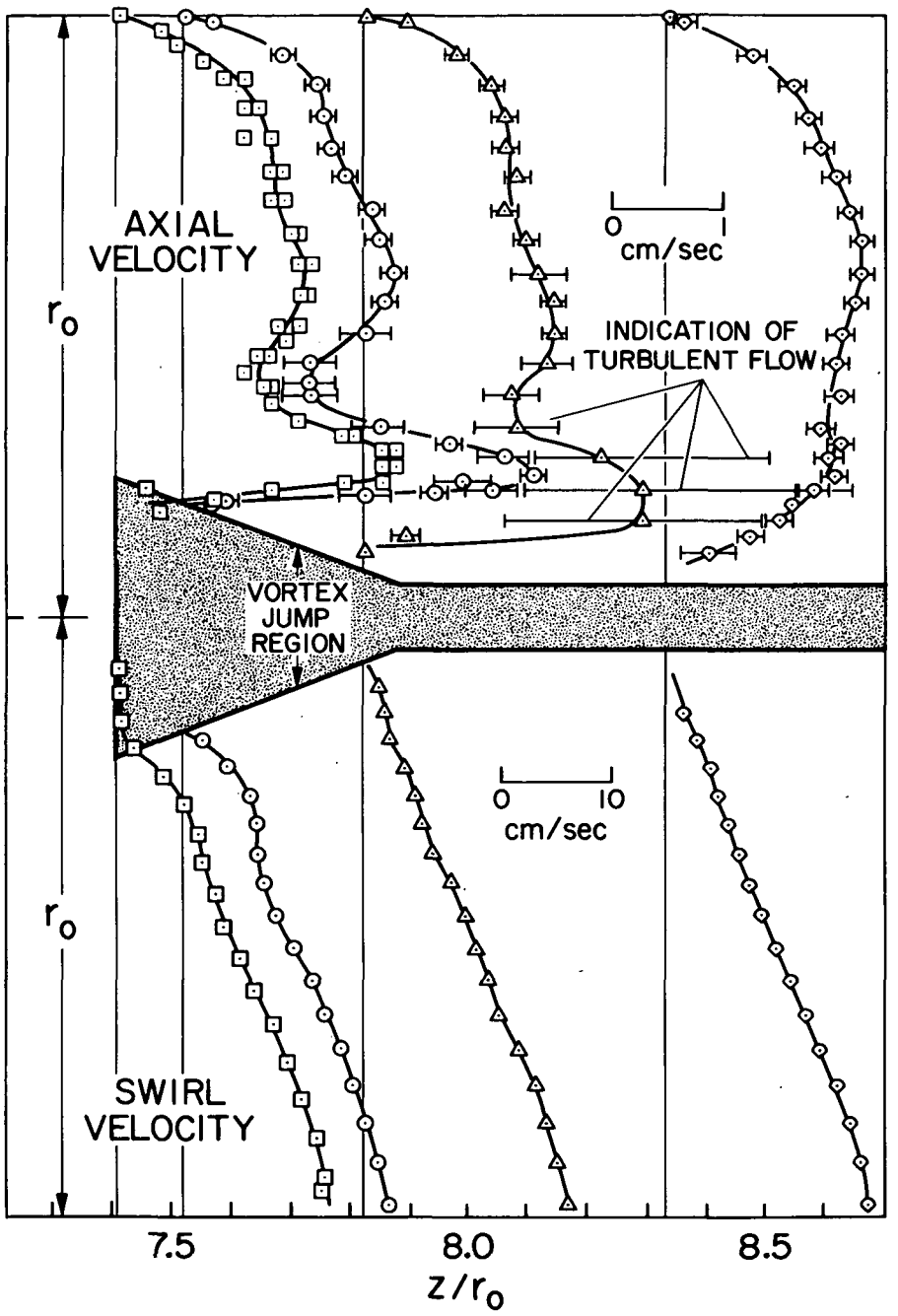
AXIAL
VELOCITY
r_o
0
cm/sec
INDICATION OF
TURBULENT FLOW
VORTEX
JUMP
REGION
0
10
cm/sec
r_o
SWIRL
VELOCITY
7.5
8.0
8.5
z/r_o

Fig. 7

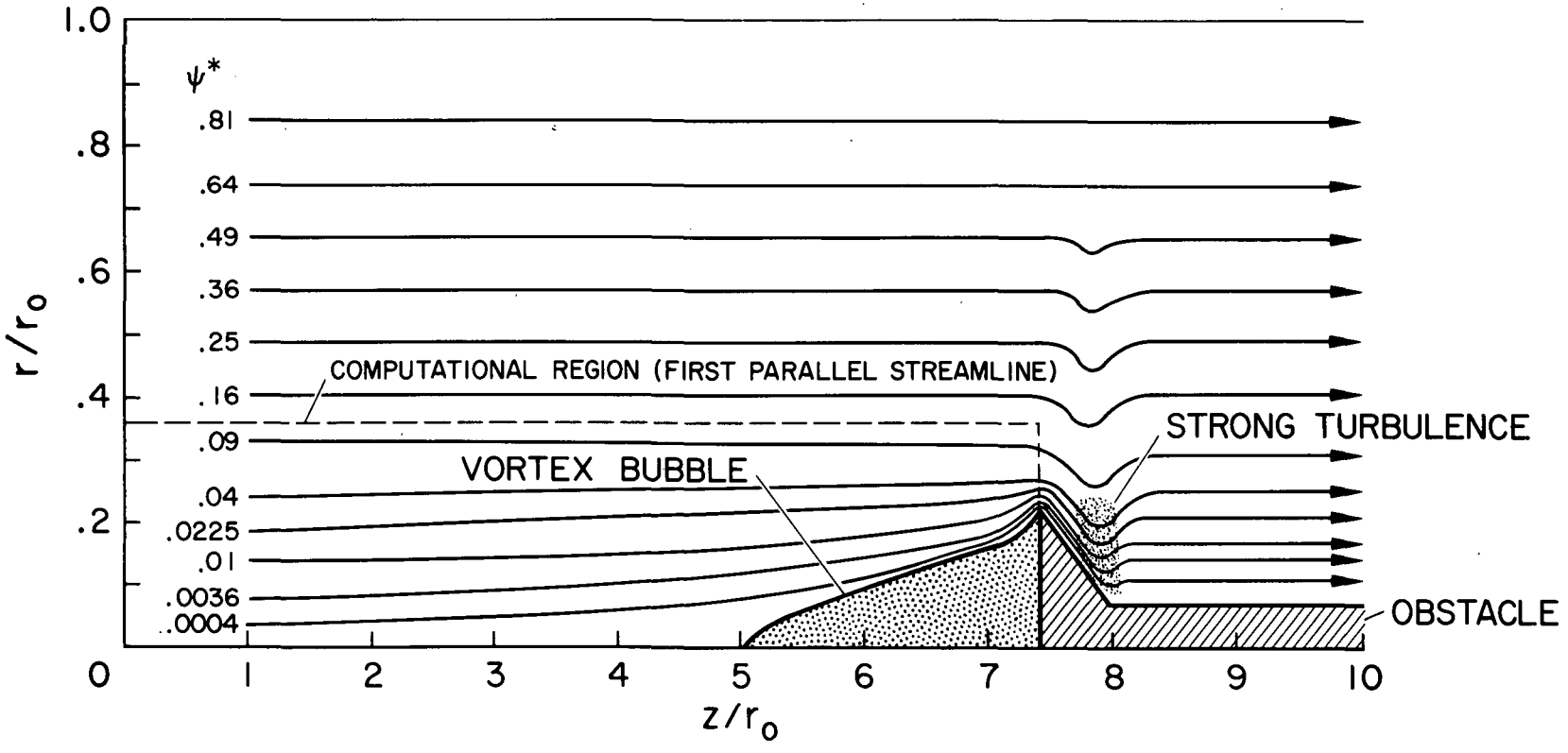
1.0
.8
.6
.4
.2
0
r/r0
ψ*
.81
.64
.49
.36
.25
.16
.09
.04
.0225
.01
.0036
.0004
COMPUTATIONAL REGION (FIRST PARALLEL STREAMLINE)
VORTEX BUBBLE
STRONG TURBULENCE
OBSTACLE
1
2
3
4
5
6
7
8
9
10
z/r0

Fig. 8

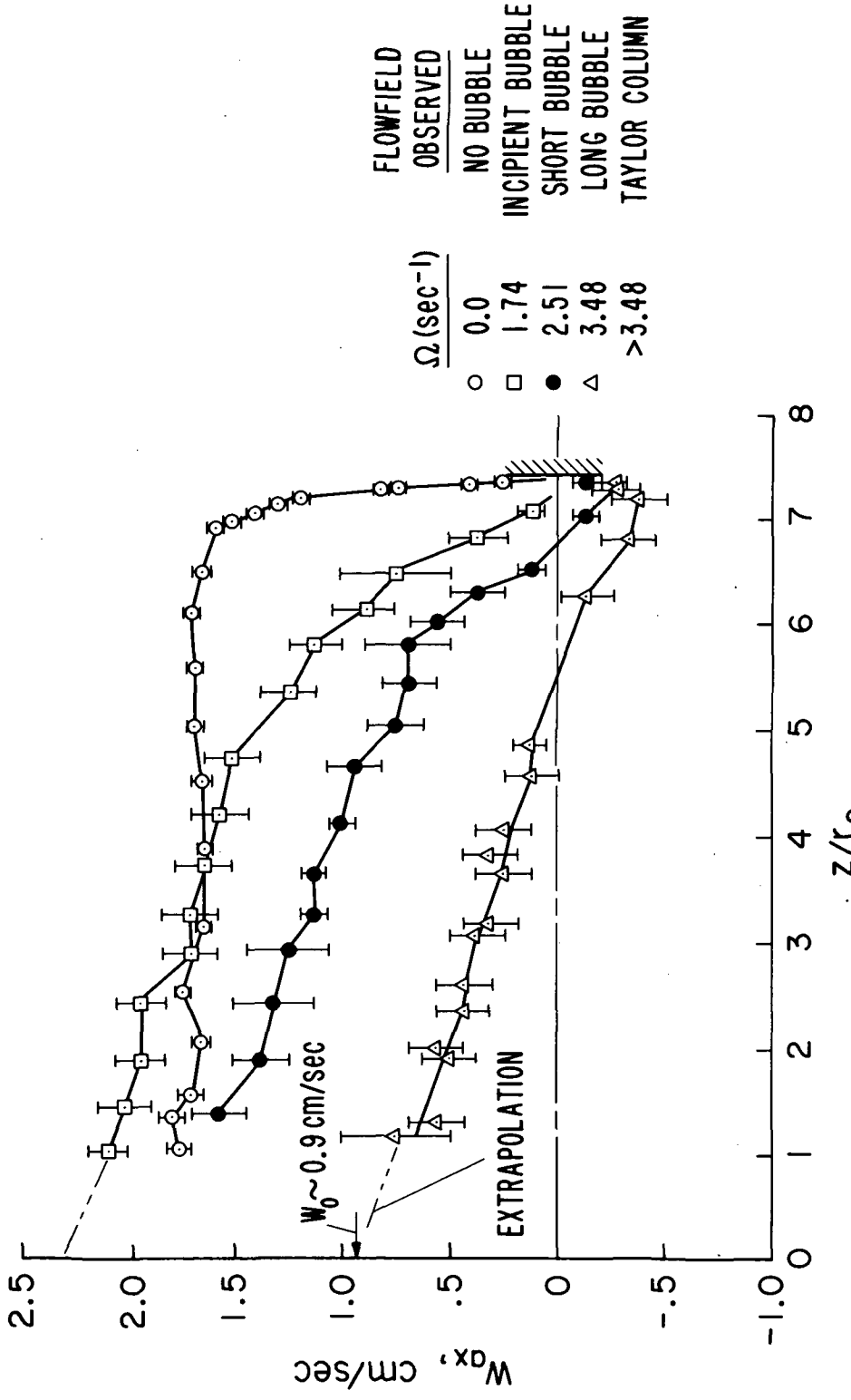
FLOWFIELD OBSERVED
NO BUBBLE
INCIPIENT BUBBLE
SHORT BUBBLE
LONG BUBBLE
TAYLOR COLUMN
Ω(sec⁻¹)
0.0
1.74
2.51
3.48
>3.48
W₀~0.9 cm/sec
EXTRAPOLATION
W_ax, cm/sec
z/r₀
2.5
2.0
1.5
1.0
.5
0
-.5
-1.0
0
1
2
3
4
5
6
7
8

Fig. 9

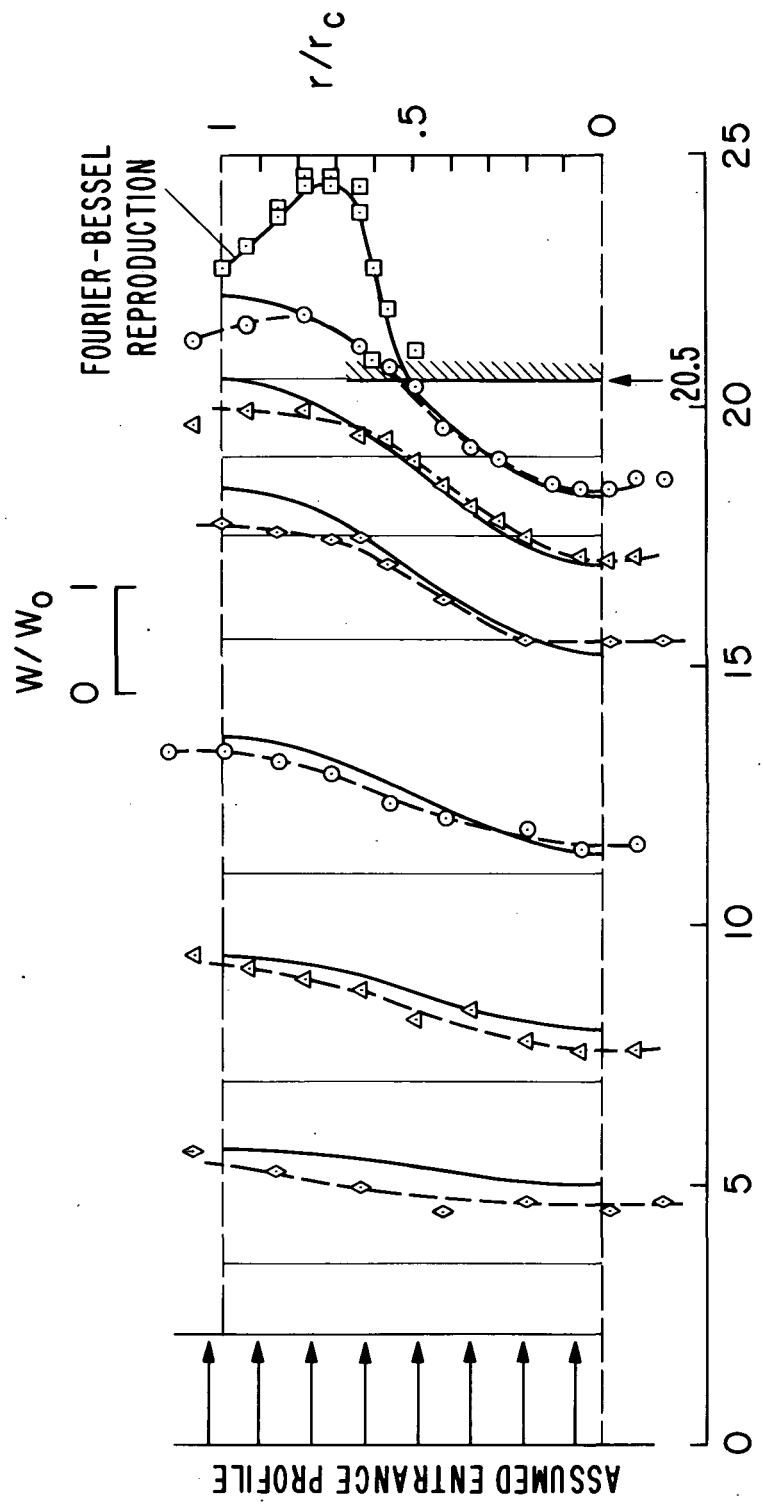
r/r_c
1
.5
0
FOURIER-BESSEL
REPRODUCTION
20.5
W/W_o
1
0
25
20
15
10
5
0
z/r_c
ASSUMED ENTRANCE PROFILE

Fig. 10

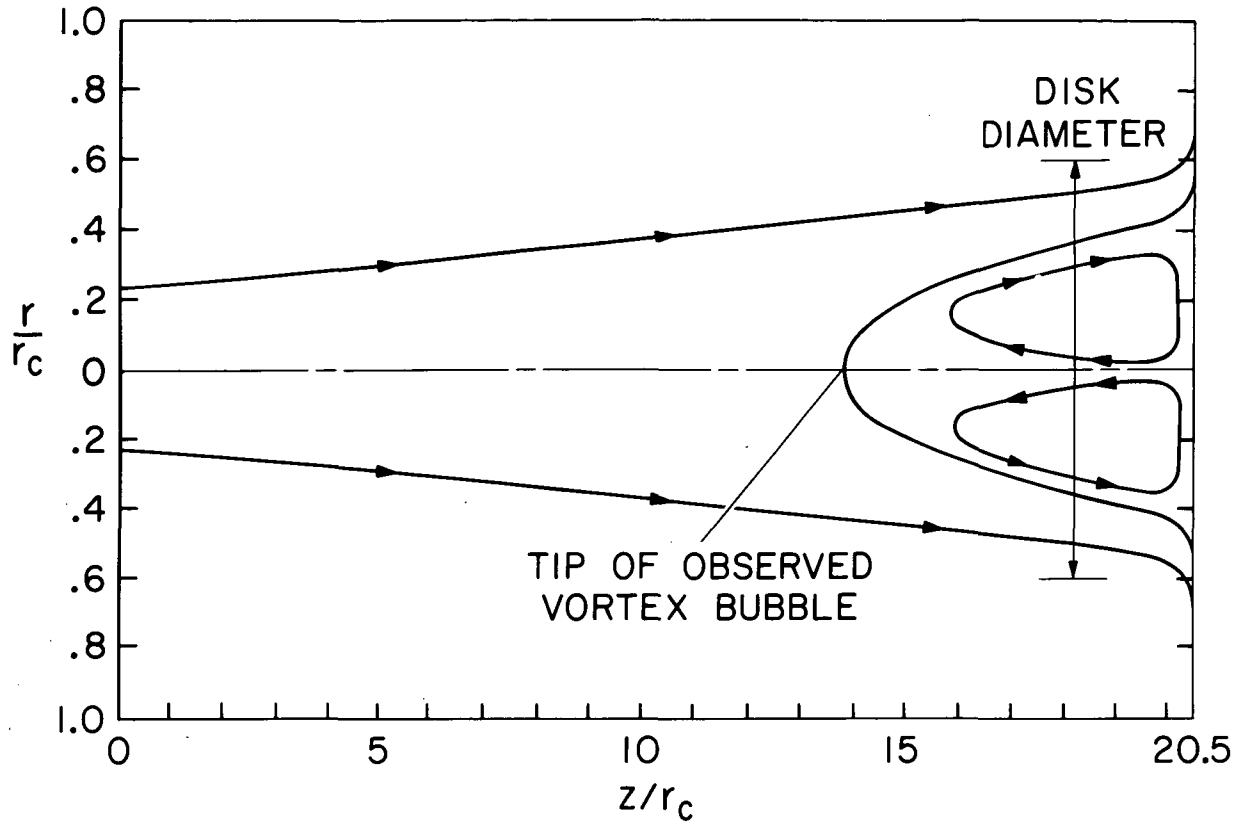
1.0
.8
.6
.4
.2
0
.2
.4
.6
.8
1.0
r/rc
0
5
10
15
20.5
z/rc
DISK
DIAMETER
TIP OF OBSERVED
VORTEX BUBBLE

Fig. 11

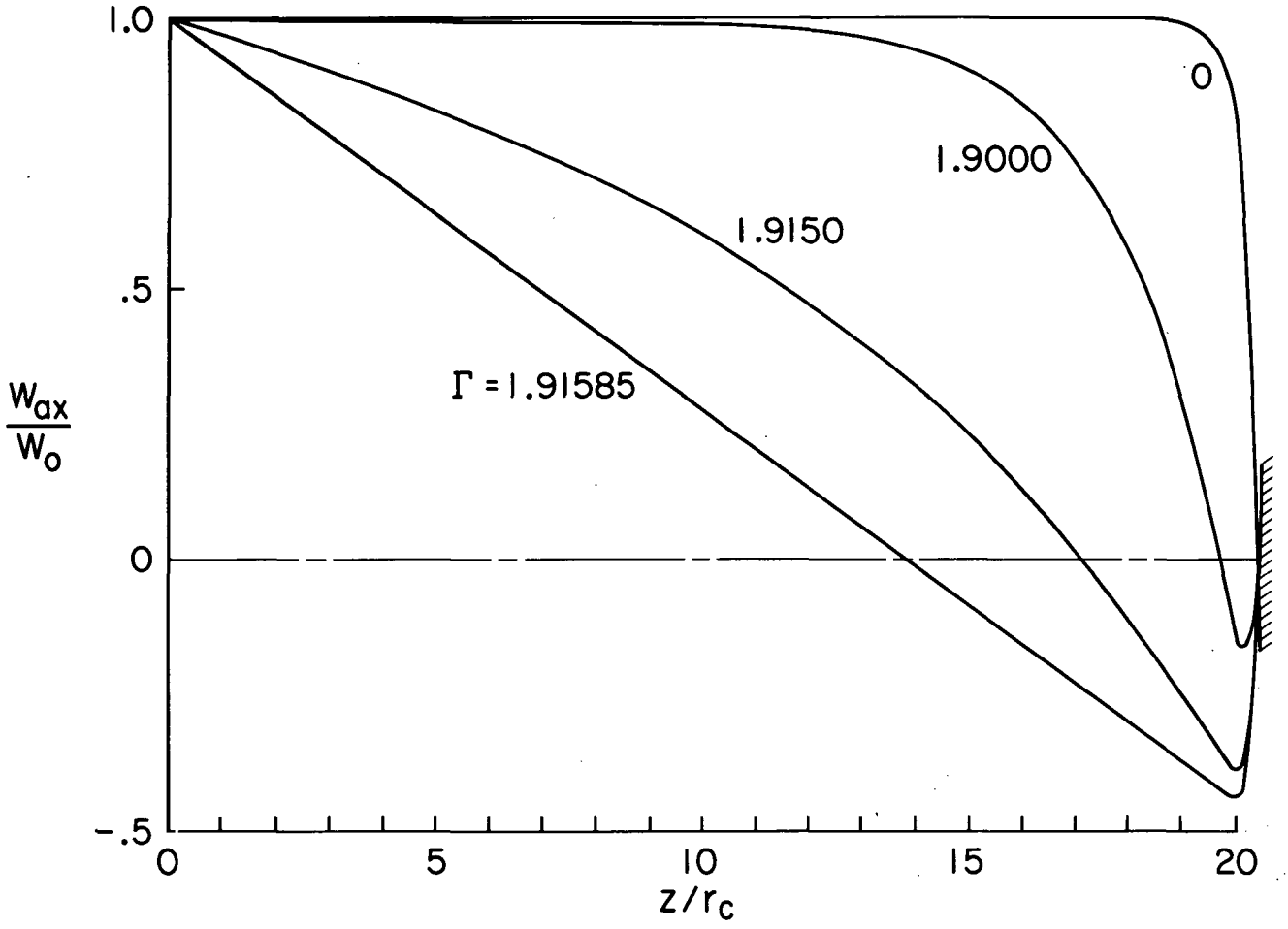

Fig. 12

NASA-Langley, 1973 —— 12 CR-2284

"The aeronautical and space activities of the United States shall be conducted so as to contribute . . . to the expansion of human knowledge of phenomena in the atmosphere and space. The Administration shall provide for the widest practicable and appropriate dissemination of information concerning its activities and the results thereof."

—NATIONAL AERONAUTICS AND SPACE ACT OF 1958

NASA SCIENTIFIC AND TECHNICAL PUBLICATIONS

TECHNICAL REPORTS: Scientific and technical information considered important, complete, and a lasting contribution to existing knowledge.

TECHNICAL NOTES: Information less broad in scope but nevertheless of importance as a contribution to existing knowledge.

TECHNICAL MEMORANDUMS: Information receiving limited distribution because of preliminary data, security classification, or other reasons. Also includes conference proceedings with either limited or unlimited distribution.

CONTRACTOR REPORTS: Scientific and technical information generated under a NASA contract or grant and considered an important contribution to existing knowledge.

TECHNICAL TRANSLATIONS: Information published in a foreign language considered to merit NASA distribution in English.

SPECIAL PUBLICATIONS: Information derived from or of value to NASA activities. Publications include final reports of major projects, monographs, data compilations, handbooks, sourcebooks, and special bibliographies.

TECHNOLOGY UTILIZATION PUBLICATIONS: Information on technology used by NASA that may be of particular interest in commercial and other non-aerospace applications. Publications include Tech Briefs, Technology Utilization Reports and Technology Surveys.

Details on the availability of these publications may be obtained from:

SCIENTIFIC AND TECHNICAL INFORMATION OFFICE

NATIONAL AERONAUTICS AND SPACE ADMINISTRATION

Washington, D.C. 20546